

# AGMA: Adaptive Gaussian Mixture Anchors for Prior-Guided Multimodal Human Trajectory Forecasting

Chao Li<sup>1</sup> Rui Zhang<sup>1</sup> Siyuan Huang<sup>2</sup> Xian Zhong<sup>1</sup> Hongbo Jiang<sup>3</sup>

## Abstract

Human trajectory forecasting requires capturing the multimodal nature of pedestrian behavior. However, existing approaches suffer from prior misalignment. Their learned or fixed priors often fail to capture the full distribution of plausible futures, limiting both prediction accuracy and diversity. We theoretically establish that prediction error is lower-bounded by prior quality, making prior modeling a key performance bottleneck. Guided by this insight, we propose **AGMA** (Adaptive Gaussian Mixture Anchors), which constructs expressive priors through two stages: extracting diverse behavioral patterns from training data and distilling them into a scene-adaptive global prior for inference. Extensive experiments on ETH-UCY, Stanford Drone, and JRDB datasets demonstrate that AGMA achieves state-of-the-art performance, confirming the critical role of high-quality priors in trajectory forecasting.

## 1. Introduction

Trajectory forecasting is a cornerstone capability for autonomous systems, enabling safe navigation in human-populated environments (Ettinger et al., 2021; Sadat et al., 2020; Floreano & Wood, 2015; Rudenko et al., 2020). The task demands predicting not only accurate future paths but also the multimodality of human behaviors (Rudenko et al., 2020).

To address this inherent multimodality, recent methods introduce auxiliary mechanisms such as destination (Mangalam et al., 2020b), patterns (Shi et al., 2023), and Gaussian distribution (Maeda & Ukita, 2023). From a Bayesian perspective (Kingma & Welling, 2013; Sohn et al., 2015), these mechanisms can be interpreted as *priors* that guide

<sup>1</sup>School of Computer Science and Artificial Intelligence, Wuhan University of Technology, Wuhan, China <sup>2</sup>Whiting School of Engineering, Johns Hopkins University, Baltimore, MD, USA

<sup>3</sup>College of Computer Science and Electronic Engineering, Hunan University, Changsha, China. Correspondence to: Chao Li <302476@whut.edu.cn>.

Preprint. February 5, 2026.

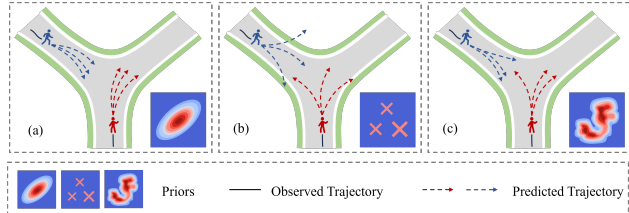


Figure 1. Qualitative comparison of priors at a three-way intersection with two agents: (a) Implicit Gaussian priors: Simple Gaussian priors collapse to a single dominant mode during training, yielding limited diversity. (b) Discrete anchor priors: Fixed discrete priors produce repetitive predictions that fail to adapt to scene-specific contexts. (c) AGMA (Ours): Adaptive Gaussian Mixture Anchors generate diverse, semantically aligned predictions through explicit, scene-aware prior construction.

the model in exploring the space of possible future trajectories (Lee et al., 2017; Gupta et al., 2018) and fundamentally drive the generation of diverse predictions. For example, at an intersection, such priors may encode typical behavioral patterns such as turning left, going straight, or turning right.

Despite the established role of priors in multimodal forecasting, recent research has focused primarily on application-driven improvements, such as scene understanding and agent interaction modeling (Shi et al., 2024; Chen et al., 2025; Bae et al., 2022). While these advances have improved overall performance, the prior mechanisms involved are often treated as fixed auxiliary components. This oversight has left their formulation and impact largely underexplored.

We identify two prevalent paradigms for handling priors in trajectory forecasting. *Implicit Gaussian priors* (Fang et al., 2025; Fu et al., 2025; Bhattacharyya et al., 2019; Mao et al., 2023a) leverage continuous latent variables sampled from certain distributions (e.g., standard Gaussians), aiming to induce diversity through stochastic sampling. These methods typically employ variational inference frameworks in which the prior is learned implicitly as a byproduct of optimizing reconstruction objectives. *Discrete anchor priors* (Fang et al., 2025; Sun et al., 2021; Chen et al., 2024; Chai et al., 2020; Phan-Minh et al., 2020), in contrast, explicitly define a finite set of behavioral modes, typically derived from dataset-level clustering (e.g., k-means on future trajectories).

Each anchor represents a prototypical trajectory pattern, and predictions are generated by selecting and refining these discrete templates.

However, Implicit Gaussian priors are prone to *mode collapse* during training (Yan et al., 2020; Nicoli et al., 2023; Dai et al., 2020)(Fig. 1a). Discrete anchor priors, while avoiding collapse through explicit mode enumeration, offer a finite set of discrete patterns, resulting in predictions confined to these limited anchors (Madjid et al., 2025).(Fig. 1b). For example, at a three-way intersection, fixed anchors may generate left-turn predictions even when the road geometry prohibits such maneuvers.

These phenomena suggest that prior knowledge plays a more central role in trajectory forecasting than previously assumed. We further examine this point through theoretical analysis (detailed in Sect. 3). We show that improving prior quality is essential to achieve accurate and diverse predictions. Despite employing different mechanisms, both existing paradigms suffer from prior misalignment: the implicit Gaussian prior collapses to average behaviors, while discrete candidate point-based priors approximate continuous behaviors in a coarse and often suboptimal manner.

Therefore, we aim to improve prior quality by addressing misalignment and validating our theoretical insights through empirical comparisons with state-of-the-art methods. To this end, we propose Adaptive Gaussian Mixture Anchors (AGMA), a prior modeling framework based on two key strategies: (1) A *batch-wise clustering autoencoder*, which clusters trajectory embeddings within each batch and decodes cluster assignments back to trajectory space, producing batch-specific priors; and (2) An *optimal transport-based distillation*, which aggregates batch priors into a global GMM using cross attention to form global priors.

Extensive experiments on three benchmarks (ETH-UCY (Lerner et al., 2007; Pellegrini et al., 2009), Stanford Drone (Robicquet et al., 2016), ego-centric JRDB (Martín-Martín et al., 2023)) confirm our thesis: AGMA achieves competitive performance, outperforming methods with complex decoders but misalignment priors.

In summary, our main contributions are as follows.

- We identify prior quality as the critical factor for multimodal trajectory forecasting through theoretical analysis. Specifically, we prove that high-quality priors are necessary for achieving accurate predictions and faithful distribution matching.
- We propose AGMA, a framework for explicitly optimizing prior quality via batch-wise clustering autoencoding and optimal transfer-based distillation, effectively mitigating prior misalignment.

- Experiments on ETH/UCY and JRDB show that AGMA achieves state-of-the-art performance, improving mADE<sub>20</sub> by 5.26% and mFDE<sub>20</sub> by 9.38% on ETH/UCY.

## 2. Related work

### 2.1. Gaussian-based Priors

A major line of multimodal forecasting approaches introduces a latent variable  $z$ , typically drawn from a Gaussian distribution, to implicitly encode the underlying behavioral patterns. Various strategies have been explored under this paradigm. Apratim et al. (Bhattacharyya et al., 2019) proposed CF-VAE using conditional normalizing flows, while Mao et al. (Mao et al., 2023a) and Fu et al. (Fu et al., 2025) improved the inference efficiency for diffusion and flow-matching models, respectively. Parallel efforts enhance interaction and context modeling to improve prediction robustness.

Despite this progress, these methods remain fundamentally constrained by the unimodal nature of their Gaussian priors. The intrinsic lack of multimodality forces models to compensate for limited diversity via increasingly complex architectures. For example, Neuralized Markov Random Field (NMRF) (Fang et al., 2025) and Trajectory-Scene-Cell (TSC) (HU & Cham, 2025) incorporate specialized decoders or interaction modules to capture richer dynamics, effectively counterbalancing the simplicity of their latent priors.

### 2.2. Mode-based Priors

In contrast, another family of approaches introduces a discrete latent variable  $z$  to explicitly represent distinct behavioral patterns, thereby directly addressing multimodality. These works typically define patterns as representative trajectory prototypes. Sun et al. (Sun et al., 2021) proposed PCCSNet, which clusters historical paths into modality sets, classifies observations into these patterns, and synthesizes the corresponding futures. Shi et al. (Shi et al., 2023) introduced TUTR, which relies on a set of pre-computed motion patterns to generate probabilistic future trajectories without post-processing.

A related branch constructs structured, data-driven latent spaces for mode representation. Bae et al. (Bae et al., 2023; 2024) applied SVD to form compact latent spaces for efficient trajectory encoding. Chen et al. (Chen et al., 2024) further advanced this direction with Mixed Gaussian Flow (MGF), which clusters training data into multimodal Gaussian priors serving as expressive base distributions for flow-based modeling.

However, whether patterns are defined as prototypes, latent

components, or clustered priors, their quantity and structure are typically fixed before training, which limits their adaptability compared to true priors. This static "one-size-fits-all" design restricts the model's ability to effectively handle diversity human motion scenes.

### 3. The Necessity of Priors

#### 3.1. Problem Formulation

Consider a scene containing  $M$  pedestrians. We denote the collection of trajectory pairs in the scene as:

$$\mathcal{S} = \{(x_j, y_j)\}_{j=1}^M, \quad x_j \in \mathbb{R}^{T_{\text{obs}} \times d}, y_j \in \mathbb{R}^{T_{\text{pred}} \times d} \quad (1)$$

where  $M$  is the number of pedestrians,  $T_{\text{obs}}$  and  $T_{\text{pred}}$  denote the observation and prediction time steps respectively, and  $d$  is the spatial dimension (typically  $d = 2$  for 2D coordinates). The trajectory forecasting task is to predict the future trajectories  $\{y_j\}_{j=1}^M$  given the observed trajectories  $\{x_j\}_{j=1}^M$ .

However, in real-world scenarios with complex interactions and diverse human intentions, predicting a single deterministic future trajectory from observations is unrealistic. Instead, the task becomes predicting a distribution over plausible future trajectories (Liang et al., 2020; Salzmann et al., 2020). To formalize this, we treat the future trajectory  $Y_j$  as a random variable taking values in the possible future trajectory space, and denote the true conditional distribution as:

$$p(Y_j | X) = p(Y_j | \{x_k\}_{k=1}^M), \quad (2)$$

which assigns probability densities to all possible future paths of pedestrian  $j$ , conditioned on the observed trajectories  $X = \{x_k\}_{k=1}^M$ .

For the discrete anchors and implicit Gaussian priors, we unify their perspectives through variable  $z$ :

$$\begin{aligned} p(Y_j | X) &= \sum_{c=1}^C \underbrace{p(Y_j | X, z_c)}_{\text{sampler}} \cdot \underbrace{p(z_c | X)}_{\text{prior}}, \quad (\text{discrete } z) \\ &\text{or} \\ p(Y_j | X) &= \int \underbrace{p(Y_j | X, z)}_{\text{sampler}} \cdot \underbrace{p(z | X)}_{\text{prior}} dz, \quad (\text{continuous } z) \end{aligned} \quad (3)$$

While Eq. (3) offers a principled view of multimodal prediction, the prior term  $p(z | X)$  remains what we concerned in this work.

#### 3.2. How Prior Matters

Trajectory prediction pursues two fundamental objectives:

**Prediction Accuracy:** Minimizing the expected distance

between predicted and ground-truth trajectories:

$$\mathcal{L}_{\text{acc}} = \mathbb{E}_{X, Y_j} \left[ \min_k \|Y_j - \hat{Y}_j^{(k)}\|_2 \right], \quad (4)$$

where  $\hat{Y}_j^{(1)}, \dots, \hat{Y}_j^{(K)}$  are  $K$  sampled predictions.

**Distribution Matching:** Aligning the predicted distribution with the true conditional distribution:

$$\mathcal{L}_{\text{dist}} = \mathbb{E}_X [\text{KL}(p(Y_j | X) \| q(Y_j | X))]. \quad (5)$$

To expose this limitation, we decompose  $\mathcal{L}_{\text{dist}}$  into prior and sampler components. Let  $q(Y_j | X)$  denote the predictive distribution produced by model  $q$ , which factorizes into a learned prior  $q(z | X)$  and a conditional sampler  $q(Y_j | X, z)$ .

**Theorem 3.1.** *For a given scene with observed trajectories  $X$  and target agent  $j$ , define the prior error and sampler error as:*

$$\epsilon_{\text{prior}}(X) = \left\| \int (p(z | X) - q(z | X)) q(Y_j | X, z) dz \right\|_1, \quad (6)$$

$$\epsilon_{\text{sample}}(X) = \left\| \int p(z | X) (p(Y_j | X, z) - q(Y_j | X, z)) dz \right\|_1, \quad (7)$$

where  $\epsilon_{\text{prior}}(X)$  measures the distributional mismatch between the true prior  $p(z | X)$  and the learned prior  $q(z | X)$ , and  $\epsilon_{\text{sample}}(X)$  quantifies the sampler's reconstruction accuracy. Then the prediction loss satisfies:

$$\mathcal{L}_{\text{dist}}(X) \geq \frac{1}{2} (\epsilon_{\text{prior}}(X) - \epsilon_{\text{sample}}(X))^2. \quad (8)$$

*Proof.* See *Supplementary Materials*.  $\square$

##### 3.2.1. STAGE 1: PRIOR LIMITS PREDICTION ACCURACY

The sampler's ability to reconstruct  $Y_j$  from latent code  $z$  is fundamentally constrained by the information content of  $z$ . By the data processing inequality:

$$I(Y_j; \hat{Y}_j | X) \leq I(Y_j; z | X), \quad (9)$$

with equality achieved only when  $z$  is a sufficient statistic for  $Y_j$  given  $X$ .

**Proposition 3.2.** *For a fixed prior  $q(z | X)$ , the sampler error is lower-bounded by:*

$$\epsilon_{\text{sample}}(X) \geq \mathcal{C}(H(Y_j | X) - I(Y_j; z | X)), \quad (10)$$

where  $\mathcal{C}(h) = \sqrt{2\sigma^2 h}$  is a monotonically increasing function,  $H(Y_j | X)$  is the conditional entropy of trajectories, and  $\sigma^2$  characterizes the noise level in trajectory distributions.

*Proof.* Consider the optimal sampler  $q^*(Y_j|X, z) = \mathbb{E}[Y_j|X, z]$  that minimizes the expected reconstruction error. The residual uncertainty satisfies:

$$H(Y_j|X, z) = H(Y_j|X) - I(Y_j; z|X) \geq 0. \quad (11)$$

By Fano's inequality for continuous variables, the mean squared reconstruction error is bounded by:

$$\mathbb{E}_{p(Y_j, z|X)} [\|Y_j - \mathbb{E}[Y_j|X, z]\|_2^2] \geq \sigma^2 H(Y_j|X, z), \quad (12)$$

where  $\sigma^2$  depends on the effective dimensionality and variance of  $Y_j$ . Converting to  $L_1$  distance via Cauchy-Schwarz and applying Pinsker's inequality:

$$\epsilon_{\text{sample}}(X) = \mathbb{E}_{p(z|X)} [\|p(Y_j|X, z) - q^*(Y_j|X, z)\|_1] \quad (13)$$

$$\geq \sqrt{2 \cdot \text{KL}(p(Y_j|X, z) \| q^*(Y_j|X, z))} \quad (14)$$

$$\geq \sqrt{2\sigma^2 H(Y_j|X, z)} \quad (15)$$

$$= \mathcal{C}(H(Y_j|X) - I(Y_j; z|X)), \quad (16)$$

where the second inequality follows from the relationship between KL divergence and entropy for Gaussian-like distributions.  $\square$

Proposition 3.2 reveals that when the prior  $q(z|X)$  fails to capture sufficient information about  $Y_j$  (i.e.,  $I(Y_j; z|X) \ll H(Y_j|X)$ ), the sampler faces an irreducible error floor determined purely by the information gap.

When the learned prior  $q(z|X)$  is informationally deficient, we have:

$$I(Y_j; z|X) < H(Y_j|X) - \delta_{\text{info}}, \quad (17)$$

for some information gap  $\delta_{\text{info}} > 0$ . In this regime, even with an optimal sampler  $q^*(Y_j|X, z) = \mathbb{E}[Y_j|X, z]$ , the sampler error remains bounded away from zero:

$$\epsilon_{\text{sample}}^{\min}(X) \geq \mathcal{C}(\delta_{\text{info}}) > 0. \quad (18)$$

*Remark 3.3.* Gradient-based optimization of  $\mathcal{L}_{\text{acc}}$  with respect to sampler parameters  $\theta_{\text{sample}}$  satisfies:

$$\lim_{t \rightarrow \infty} \epsilon_{\text{sample}}^{(t)}(X) = \epsilon_{\text{sample}}^{\min}(X) = H(Y_j|X) - I(Y_j; z|X), \quad (19)$$

where  $t$  indexes training iterations. This plateau is reached when the sampler has extracted all available information from  $z$ , leaving only the irreducible uncertainty  $H(Y_j|X, z)$ .

### 3.2.2. STAGE 2: PRIOR LIMITS DISTRIBUTION MATCHING

Combining Theorem 3.1 with the sampler performance ceiling from Proposition 3.2, we establish the necessity of high-quality priors:

**Corollary 3.4.** *For any target distribution matching error  $\delta > 0$ , achieving  $\mathcal{L}_{\text{dist}}(X) < \delta$  requires the prior error to satisfy when  $\epsilon_{\text{sample}} < \epsilon_{\text{prior}}$ :*

$$\epsilon_{\text{prior}}(X) < \sqrt{2\delta} + \epsilon_{\text{sample}}^{\min}(X), \quad (20)$$

where  $\epsilon_{\text{sample}}^{\min}(X) = \mathcal{C}(H(Y_j|X) - I(Y_j; z|X))$  is the information-theoretic lower bound from Eq. (10).

*Proof.* See *Supplementary Materials*.  $\square$

## 4. Methodology

### 4.1. Overview

According to Theorem 3.1 and Corollary 3.4, minimizing prediction error fundamentally requires minimizing the mismatch between learned prior  $q(z|X)$  and true prior  $p(z|X)$ . To validate this insight, we propose AGMA, a two-stage framework that explicitly model priors:

**Stage 1: Batch Prior Extraction (§4.2).** We encode complete trajectories and apply graph-based clustering to discover future trajectory patterns. Clustering is optimized by decoding cluster assignments back to trajectories, maximizing  $I(Y_j; z|X)$  through reconstruction, generating batch-level priors  $q(z|X^{(b)}, Y^{(b)})$  that preserve long-tail patterns.

**Stage 2: Global Prior Distillation (§4.3).** Batch-discovered patterns are distilled into a global GMM through optimal transport, with cross-attention selecting relevant components and forming  $p(z|X)$  in global.

To isolate the effect of prior quality, we employ a simple MLP decoder, demonstrating that strong performance stems from expressive priors rather than complex samplers.

### 4.2. Batch Prior Extraction

The Proposition 3.2 reveals that the performance of the sampler is fundamentally limited by  $I(Y_j; z|X)$ . To construct informative priors, we discover behavioral patterns through graph clustering, then optimize the clustering to maximize mutual information by decoding cluster assignments back to trajectories.

For each training batch  $\mathcal{B} = \{S^{(b)}\}_{b=1}^{B_{\text{batch}}}$ , where  $S^{(b)}$  denotes a scene containing  $M^{(b)}$  agents, we collect all agent trajectories across scenes:

$$\mathcal{B}_{\text{agents}} = \bigcup_{b=1}^{B_{\text{batch}}} \{(x_{b,j}, y_{b,j})\}_{j=1}^{M^{(b)}}, \quad (21)$$

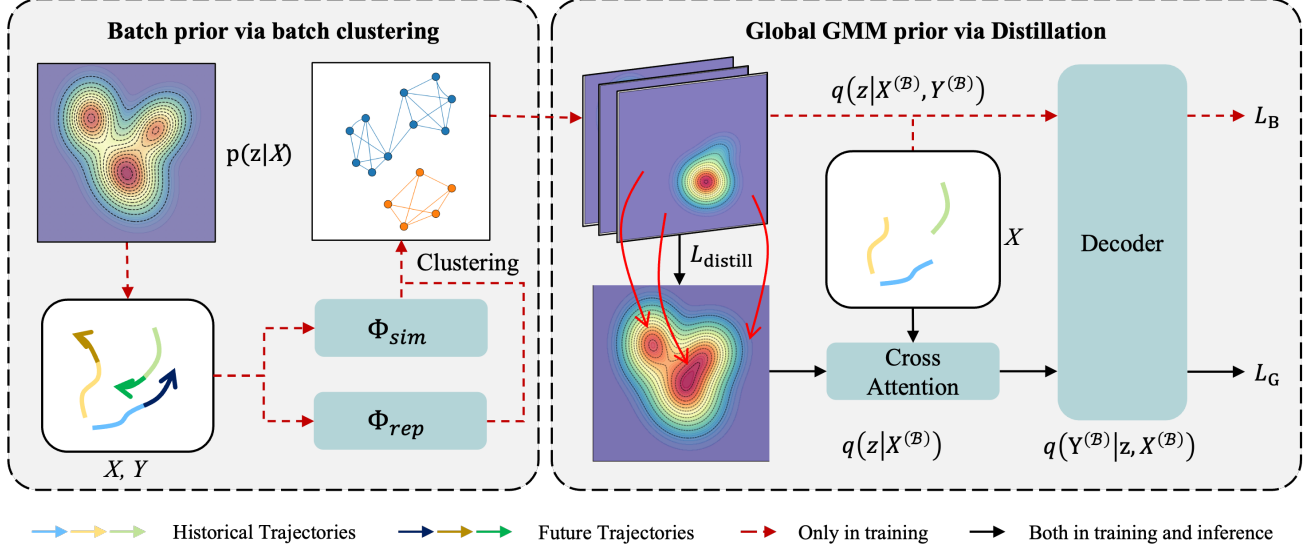


Figure 2. AGMA architecture. **Left:** Graph-based clustering discovers behavioral patterns within each batch, forming batch-level GMM priors. **Right:** Optimal transport distills batch priors into a global GMM, refined via trajectory prediction with a shared decoder.

where  $(x_{b,j}, y_{b,j})$  denotes the trajectory pair of agent  $j$  in scene  $b$ . The total number of agents in the batch is  $N_{\text{batch}} = \sum_{b=1}^{B_{\text{batch}}} M^{(b)}$ .

We extract trajectory representations using two encoders  $\Phi_{\text{past}}$  and  $\Phi_{\text{full}}$  that share the same architecture: temporal convolutional layers and GRU units first encode the input into time-dependent features, which are then processed by a self-attention layer to capture socially-aware representations. For each agent  $(b, j)$  in the batch:

$$\mathbf{f}_{b,j}^{\text{past}} = \Phi_{\text{past}}(x_{b,j}), \mathbf{f}_{b,j}^{\text{full}} = \Phi_{\text{full}}(x_{b,j}, y_{b,j}) \in \mathbb{R}^d. \quad (22)$$

Recall that  $\mathbf{f}_{b,j}^{\text{past}}$  encodes the observed context while  $\mathbf{f}_{b,j}^{\text{full}}$  encodes the complete trajectory.

We employ graph-based clustering that explicitly models behavioral similarity in trajectory space across all agents in the batch. For each agent  $(b, j)$ , we compute dual projections of its full trajectory embedding via MLPs:

$$\mathbf{s}_{b,j} = \Phi_{\text{sim}}(\mathbf{f}_{b,j}^{\text{full}}), \quad \mathbf{r}_{b,j} = \Phi_{\text{rep}}(\mathbf{f}_{b,j}^{\text{full}}), \quad (23)$$

where  $\mathbb{I}[\cdot]$  denotes the indicator function. Two agents are connected if they exhibit high similarity ( $\tilde{S} > \theta_{\text{sim}}$ ) and low repulsion ( $\tilde{R} < \theta_{\text{rep}}$ ), indicating membership in the same behavioral mode. We enable end-to-end training of the thresholds via the Straight-Through Estimator (Bae et al., 2022) (details in Appendix B).

The graph adjacency matrix is constructed using learnable thresholds  $\theta_{\text{sim}}$  and  $\theta_{\text{rep}}$ . For agents  $(b, j)$  and  $(b', j')$ :

$$A_{(b,j),(b',j')} = \mathbb{I}[\tilde{S}_{(b,j),(b',j')} > \theta_{\text{sim}}] \wedge \mathbb{I}[\tilde{R}_{(b,j),(b',j')} < \theta_{\text{rep}}], \quad (24)$$

where  $\mathbb{I}[\cdot]$  denotes the indicator function, and differentiation through discrete thresholding is enabled through the Gumbel softmax (Jang et al., 2017) (details in Appendix C). Two agents are connected if they exhibit high similarity and low repulsion, indicating membership in the same behavioral mode.

The Connected-component analysis on graph  $A$  partitions all agents in the batch into mode clusters  $\{\mathcal{I}_k\}_{k=1}^{N_{\text{patterns}}}$ . For each cluster  $k$  with cardinality  $n_k = |\mathcal{I}_k|$ , we estimate a Gaussian component as follows:

$$\pi_{B,k} = \frac{n_k}{N_{\text{batch}}}, \quad \boldsymbol{\mu}_{B,k} = \frac{1}{n_k} \sum_{(b,j) \in \mathcal{I}_k} \mathbf{f}_{b,j}^{\text{full}}, \quad (25)$$

$$\boldsymbol{\sigma}_{B,k}^2 = \frac{1}{\max(n_k - 1, 1)} \sum_{(b,j) \in \mathcal{I}_k} (\mathbf{f}_{b,j}^{\text{full}} - \boldsymbol{\mu}_{B,k})^{\odot 2}. \quad (26)$$

Aggregating all clusters yields the batch prior in GMM form:

$$q(z|X^{(B)}, Y^{(B)}) = \sum_{k=1}^{N_{\text{patterns}}} \pi_{B,k} \mathcal{N}(z; \boldsymbol{\mu}_{B,k}, \text{diag}(\boldsymbol{\sigma}_{B,k}^2)), \quad (27)$$

which serves as an approximation of the true prior  $p(z|X)$  restricted to the current batch.

### 4.3. Global Prior Distillation

We parameterize a global prior as a GMM with  $K_g$  components in the latent space  $z$ :

$$\text{GMM}_{\text{global}} = \{(\pi_g, \boldsymbol{\mu}_g, \boldsymbol{\Sigma}_g)\}_{g=1}^{K_g}, \quad (28)$$

where  $\boldsymbol{\pi} = (\pi_1, \dots, \pi_{K_g})$  are the base mixture weights and  $\boldsymbol{\Sigma}_g = \text{diag}(\boldsymbol{\sigma}_g^2)$  are diagonal covariances.

To construct the context-conditioned prior  $q_\theta(z|x)$ , we employ a cross-attention mechanism that selects and reweights components from the GMM<sub>global</sub> based on the observed trajectories. Specifically, given the past trajectory feature  $\mathbf{f}_{b,j}^{\text{past}} = \Phi_{\text{past}}(x_{b,j})$  as the query and the global component centers  $\{\boldsymbol{\mu}_g\}_{g=1}^{K_g}$  as keys, we compute attention scores:

$$a_{b,j,g} = \text{CrossAttention}(\mathbf{f}_{b,j}^{\text{past}}, \{\boldsymbol{\mu}_g\}_{g=1}^{K_g})_g, \quad g = 1, \dots, K_g, \quad (29)$$

where  $a_{b,j,g} \in [0, 1]$  and  $\sum_{g=1}^{K_g} a_{b,j,g} = 1$ .

The context-dependent prior for agent  $(b, j)$  is then formed as a reweighted sub-GMM:

$$q_\theta(z|x_{b,j}) = \sum_{g=1}^{K_g} a_{b,j,g} \mathcal{N}(z | \boldsymbol{\mu}_g, \boldsymbol{\Sigma}_g), \quad (30)$$

where the attention weights  $a_{b,j,g}$  dynamically emphasize patterns relevant to the observed trajectory  $x_{b,j}$ .

#### 4.4. Sampler for Prior

Given a past trajectory feature  $\mathbf{f}_{b,j}^{\text{past}}$  for agent  $j$  in scene  $b$  and a latent mode code  $\mathbf{z}_{b,j}^{(n)}$ , we decode future trajectories through a shared MLP decoder  $D_\phi$ :

$$\hat{Y}_{b,j}^{(n)} = D_\phi(\mathbf{f}_{b,j}^{\text{past}}, \mathbf{z}_{b,j}^{(n)}), \quad n = 1, \dots, N, \quad (31)$$

producing  $N$  candidate future trajectories per agent. The decoder  $D_\phi$  is shared across both the batch prior extraction (§4.2) and the global prior inference stages.

#### 4.5. Training and Inference

We jointly optimize three components: (1) batch-level clustering quality, (2) global prior distillation, and (3) trajectory reconstruction accuracy.

For each agent  $(b, j)$  assigned to cluster  $c_{b,j}$ , we sample latent codes from its cluster's Gaussian:

$$\mathbf{z}_{b,j,B}^{(n)} \sim \mathcal{N}(\boldsymbol{\mu}_{B,c_{b,j}}, \boldsymbol{\Sigma}_{B,c_{b,j}}), \quad \hat{Y}_{b,j,B}^{(n)} = D_\phi(\mathbf{f}_{b,j}^{\text{past}}, \mathbf{z}_{b,j,B}^{(n)}), \quad (32)$$

and minimize best-of- $N$  ADE (Fang et al., 2025):

$$\mathcal{L}_B = \frac{1}{N_{\text{batch}}} \sum_{b,j} \min_n \text{ADE}(\hat{Y}_{b,j,B}^{(n)}, Y_{b,j}). \quad (33)$$

We align the cross-attention-weighted global GMM with batch priors via entropic optimal transport:

$$\mathcal{L}_{\text{distill}} = \min_{\mathbf{P}} \langle \mathbf{P}, \mathbf{C} \rangle + \varepsilon H(\mathbf{P}), \quad \text{s.t.} \quad \mathbf{P}^\top \mathbf{1} = \bar{\mathbf{a}}, \quad \mathbf{P}^\top \mathbf{1} = \boldsymbol{\beta}_B, \quad (34)$$

where  $\bar{\mathbf{a}}$  are batch-averaged attention weights,  $\boldsymbol{\beta}_B$  are batch prior weights, and  $C_{gk} = W_2^2(\mathcal{N}(\boldsymbol{\mu}_g, \boldsymbol{\Sigma}_g), \mathcal{N}(\boldsymbol{\mu}_{B,k}, \boldsymbol{\Sigma}_{B,k}))$  measures Wasserstein distance (Panaretos & Zemel, 2019) between global and batch components.

We sample from the attention-weighted global prior and decode:

$$g \sim \text{Cat}(\mathbf{a}_{b,j}), \quad \mathbf{z}_{b,j,G}^{(n)} \sim \mathcal{N}(\boldsymbol{\mu}_g, \boldsymbol{\Sigma}_g), \quad \mathcal{L}_G = \frac{1}{N_{\text{batch}}} \sum_{b,j} \min_n \text{ADE}(\hat{Y}_{b,j,G}^{(n)}, Y_{b,j}). \quad (35)$$

The total objective is:

$$\mathcal{L}_{\text{total}} = \mathcal{L}_B + \mathcal{L}_G + \lambda \mathcal{L}_{\text{distill}}. \quad (36)$$

At test time, we use only the global prior. For each agent, cross-attention selects relevant GMM components based on  $\mathbf{f}^{\text{past}}$ , we sample  $\mathbf{z}^{(n)} \sim q_\theta(z|x)$ , and decode via  $D_\phi$  to produce  $N$  diverse predictions.

## 5. Experimental Results

We conduct extensive experiments to validate the effectiveness of the proposed AGMA framework. We first introduce the benchmark datasets and evaluation metrics (see §5.1), followed by theory-guided ablation studies and quantitative comparisons with state-of-the-art methods (see §5.3).

### 5.1. Datasets and Metrics

**Datasets.** We evaluate AGMA on three pedestrian trajectory benchmarks covering diverse interaction scenarios:

**ETH-UCY** (Pellegrini et al., 2009; Lerner et al., 2007) contains five subsets (ETH, HOTEL, UNIV, ZARA1, ZARA2). Following (Gupta et al., 2018), we use leave-one-out cross-validation, predicting 12 future frames (4.8s) from 8 observed frames (3.2s).

**Stanford Drone (SDD)** (Robicquet et al., 2016) provides bird's-eye view trajectories on a university campus. We predict 12 frames (4.8s) from 8 frames (3.2s) and report metrics in both pixel and meter units.

**JRDB** (Martín-Martín et al., 2023) is a large-scale egocentric dataset recorded by a social robot. We follow the official train-validation-test split, predicting 12 frames from 9 frames at 2.5 FPS. Trajectories are transformed to global coordinates using provided odometry. To address the validation-test leakage issue identified in (Fang et al., 2025), we strictly separate validation (for hyperparameter tuning) and test sets (for final evaluation only).

**Evaluation Metrics.** We report Average Displacement Error (ADE) and Final Displacement Error (FDE). For

Table 1. Quantitative results on the ETH-UCY dataset. We report mADE<sub>20</sub>/mFDE<sub>20</sub> (m). Best **bold**, second-best underlined.

Method	Venue	ETH		HOTEL		UNIV		ZARA1		ZARA2		AVG	
		mADE <sub>20</sub>	mFDE <sub>20</sub>										
Trajectron++	ECCV'20	0.61	1.03	0.32	0.55	0.37	0.70	0.29	0.53	0.25	0.45	0.37	0.65
PECNET	ECCV'20	0.64	1.13	0.22	0.38	0.35	0.57	0.25	0.45	0.18	0.31	0.33	0.57
GP-Graph	ECCV'22	0.43	0.63	0.18	0.30	0.25	0.48	0.23	0.45	0.18	0.35	0.25	0.44
VIKT	TITS'23	0.30	0.51	0.13	0.25	0.23	0.51	0.21	0.44	0.14	0.30	0.20	0.40
TUTR	ICCV'23	0.45	0.67	0.14	0.20	0.24	0.44	0.19	0.36	0.15	0.28	0.23	0.39
EigenTraj	ICCV'23	0.36	0.53	0.12	0.19	0.24	<b>0.34</b>	0.19	0.33	<u>0.14</u>	0.24	0.21	0.33
SocialCircle	CVPR'24	0.27	0.42	0.13	<u>0.16</u>	0.29	0.51	0.19	0.33	<u>0.14</u>	0.25	0.20	0.33
SingularTraj	CVPR'24	0.35	0.42	0.13	0.19	0.25	0.44	0.19	0.32	<u>0.15</u>	0.25	0.21	0.32
MGF	NIPS'24	0.39	0.59	0.13	0.20	<b>0.21</b>	0.39	<b>0.17</b>	<b>0.29</b>	<u>0.14</u>	0.24	0.21	0.34
MoFlow	CVPR'25	0.40	0.57	0.12	0.18	<u>0.23</u>	0.40	<b>0.17</b>	0.30	<b>0.13</b>	<b>0.23</b>	0.21	0.34
NMRF	ICLR'25	<u>0.26</u>	<u>0.37</u>	<u>0.11</u>	0.17	0.28	0.49	<b>0.17</b>	0.30	<u>0.14</u>	0.25	<u>0.19</u>	<u>0.32</u>
AGMA (Ours)		<b>0.24</b>	<b>0.35</b>	<b>0.10</b>	<b>0.15</b>	0.25	0.44	<b>0.17</b>	<b>0.29</b>	<u>0.14</u>	<b>0.23</b>	<b>0.18</b>	<b>0.29</b>

 Table 2. Comparison on SDD. We report mADE<sub>20</sub>/mFDE<sub>20</sub> (m). Best **bold**, second-best underlined.

Method	Venue	mADE <sub>20</sub>	mFDE <sub>20</sub>
TUTR	ICCV'23	7.76	12.69
EigenTraj	ICCV'23	8.05	13.25
MGF	NeurIPS'24	7.74	12.07
MoFlow	CVPR'25	7.66	12.39
NMRF	ICLR'25	<b>7.20</b>	11.29
AGMA (Ours)		<u>7.23</u>	<b>10.92</b>

 Table 3. Comparison on JRDB. We report mADE<sub>20</sub>/mFDE<sub>20</sub> (m). Best **bold**, second-best underlined.

Method	Venue	mADE <sub>20</sub>	mFDE <sub>20</sub>
LED	CVPR'23	0.18	0.28
NMRF	ICLR'25	<u>0.17</u>	0.27
AGMA (Ours)		<b>0.15</b>	<b>0.23</b>

multimodal prediction, we use minimum-of-20 metrics (mADE<sub>20</sub>/mFDE<sub>20</sub>), which measure the best prediction among 20 samples (Mangalam et al., 2020a; Mao et al., 2023b).

## 5.2. Implementation Details

Due to space constraints, we report only key hyperparameters mentioned in § 4. Complete Implementation Details are provided in the Supplementary Materials D. The learnable thresholds are initialized as  $\theta_{\text{sim}} = 0.7$  and  $\theta_{\text{rep}} = 0.3$ . For differentiable thresholding, we use the Gumbel-Softmax temperature  $\tau = 0.1$ . The global GMM contains  $K_g = 1000$  components. For entropic optimal transport, the Sinkhorn temperature is set to  $\varepsilon = 0.1$ . The distillation weight in the total objective is  $\lambda = 0.1$ .

## 5.3. Main Results

We conduct comprehensive studies to answer two core research questions that validate our theoretical framework and

method implementation.

**RQ1: Can Prior Modeling Improve Performance?** Recall from Section 3.2 that our theoretical analysis decomposes the prediction error into two sources: prior mismatch and sampler error. Theorem 1 predicts that the prior term plays a significant role when the generator is reasonably expressive, suggesting that improving  $p(z|X)$  can be effective alongside refining  $p(Y|z, X)$ . We validate this prediction through comprehensive experiments across three datasets, as shown in Table 1, Table 2 and Table 3

These results conclusively validate our theoretical framework: by explicitly minimizing the prior mismatch through batch clustering and global distillation with a relatively poor sampler  $p(Y|z, X)$ , AGMA gains the consistent improvements across diverse datasets demonstrate that: (1) prior quality  $p(z|X)$  is a dominant factor in prediction accuracy, validating our theoretical analysis in Section 3.2, and (2) AGMA’s adaptive prior construction effectively minimizes the prior misalignment, thereby reducing the  $\mathcal{L}$  identified in Theorem 1.

**RQ2: How AGMA work?** We evaluate three variants by removing each loss term. Removing  $\mathcal{L}_B$  (w/o  $\mathcal{L}_B$ ) constructs the batch prior  $q_B$  purely from clustering without prediction-driven refinement. Removing  $\mathcal{L}_G$  (w/o  $\mathcal{L}_G$ ) allows the global prior  $q$  to learn only via distillation from batch priors, with no direct supervision. Removing  $\mathcal{L}_{\text{distill}}$  (w/o Distill) trains batch and global priors independently without distillation.

Our ablation study reveals the importance of each loss component.  $\mathcal{L}_G$  proves most critical: removing it causes the largest performance degradation, with ADE increasing by 18% and FDE by 22% on average, and even more dramatically on UNIV (+42% ADE, +46% FDE). Without direct supervision, the global prior degenerates into a smoothed replica of imperfect batch priors and loses its self-correction

Table 4. Ablation study on the ETH-UCY dataset. We report mADE<sub>20</sub>/mFDE<sub>20</sub> (m). Best results are highlighted in **bold**.

Method	ETH		HOTEL		UNIV		ZARA1		ZARA2		AVG	
	ADE	FDE										
w/o $\mathcal{L}_B$ .	0.27	0.40	0.11	0.15	0.30	0.51	0.18	0.30	0.15	0.25	0.20	0.32
w/o $\mathcal{L}_G$ .	0.26	0.36	0.11	0.15	0.43	0.82	0.18	0.30	0.14	0.23	0.22	0.37
w/o Distill	0.27	0.38	0.11	0.15	0.27	0.45	0.19	0.33	0.14	0.23	0.20	0.31
AGMA (Ours)	<b>0.25</b>	<b>0.36</b>	<b>0.10</b>	<b>0.15</b>	<b>0.25</b>	<b>0.44</b>	<b>0.17</b>	<b>0.29</b>	<b>0.14</b>	<b>0.23</b>	<b>0.18</b>	<b>0.29</b>

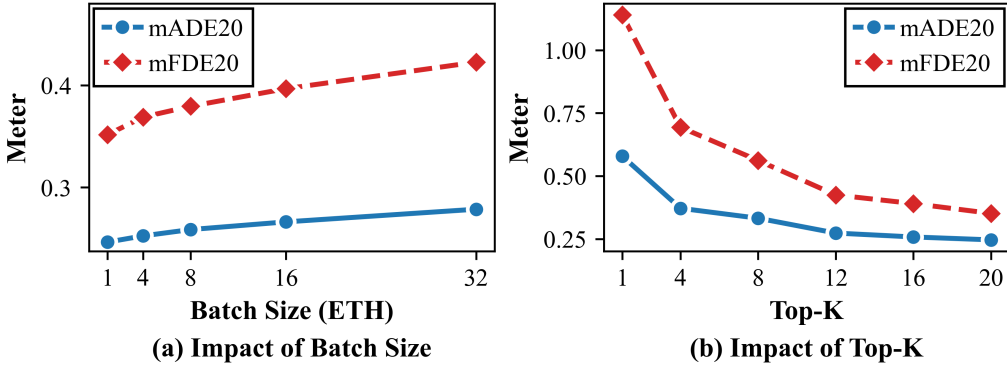


Figure 3. **Sensitivity to batch size and Top-K.** (a) Performance degrades with larger batches, demonstrating that finer batch subdivision better captures localized priors and prevents over-smoothing of the global distribution. (b) Minimal sensitivity to  $K$  validates that our model avoids overfitting  $p(Y|z, X)$  to compensate for collapsed  $p(z|X)$ —the learned prior remains informative across sampling budgets, confirming effective prior learning without mode collapse. Results on ETH dataset.

capability, confirming our theoretical analysis that once  $q \neq p$ , the generator cannot compensate (Section 3.2).  $\mathcal{L}_B$  plays a crucial refinement role: its removal increases ADE by 10% and FDE by 9%, demonstrating that while clustering alone captures trajectory diversity, it lacks accuracy-driven feedback and produces noisy mode estimates. Finally, distillation loss prevents mode collapse: without  $\mathcal{L}_{\text{distill}}$ , the global prior fails to effectively aggregate batch-level knowledge, resulting in redundant or collapsed patterns (ADE +10%, FDE +6.5%).

We further investigate the impact of batch size and top-K sampling on AGMA’s performance (Figure 3(a)). As batch size increases from 1 to 32, both ADE and FDE increase consistently. This validates our prior batch subdivision enables more accurate prior estimation  $q_B$ , preventing the global prior  $q$  from over-averaging diverse trajectory patterns into a single smoothed distribution. Larger batches, while computationally efficient, fail to capture more complete prior.

The top-K ablation reveals an expected trade-off inherent to our design philosophy. As shown in Figure 3(b), prediction error decreases consistently as  $K$  increases from 1 to 20. This behavior directly stems from our modeling priorities: AGMA is designed to investigate the relative importance of learning a high-quality prior  $p(z|X)$  versus learning a high-capacity sampler  $p(Y|z, X)$ .

Importantly, however, the steady improvement with  $K$  also validates that AGMA avoids a critical failure mode: mode collapse where the decoder  $p(Y|z, X)$  bypasses the prior and directly maps context  $X$  to outputs, as discussed in Section 3.2. If such collapse occurred, the prior would become uninformative and performance would plateau regardless of  $K$ . The observed consistent gains demonstrate that the learned prior  $p(z|X)$  genuinely encodes diverse, meaningful patterns, confirming the effectiveness of our prior learning framework.

## 6. Conclusion

In this work, we present a study on the role of priors in multimodal human trajectory forecasting. We identify *prior quality* as the critical factor for multimodal trajectory forecasting, proving that both prediction accuracy and distribution fidelity are lower-bounded by prior mismatch  $\epsilon_{\text{prior}}(X)$ . To validate this finding, we propose AGMA, which explicitly optimizes priors through batch prior extraction and global prior distillation. Experiments on ETH-UCY, SDD, and JRDB demonstrate that AGMA achieves state-of-the-art performance, with 5.26% improvement in mADE<sub>20</sub> and 9.38% in mFDE<sub>20</sub> on ETH-UCY, confirming that prior optimization is an effective way for advancing multimodal trajectory prediction.

## Impact Statement

This work advances trajectory prediction for autonomous systems through principled prior modeling. We discuss key societal considerations below.

**Positive Impact.** Our theoretical framework demonstrates that prior quality fundamentally limits prediction performance, identifying prior optimization as the critical factor for improving multimodal trajectory prediction.

**Key Limitations and Risks.** AGMA represents an initial attempt to explicitly optimize prior quality in trajectory prediction. While our method achieves strong performance on standard benchmarks, it has inherent limitations that practitioners must consider.

AGMA’s design focuses on optimizing prior quality from observed trajectories. However, it has limited capacity for modeling complex agent-agent interactions, particularly in scenarios where observed trajectories alone provide insufficient information to disambiguate future interaction details. When the observation history  $X$  does not contain discriminative cues for highly divergent interaction patterns (e.g., yielding vs. crossing in ambiguous right-of-way situations), AGMA’s context-conditioned prior  $q(z|X)$  may fail to capture the true multimodal distribution. In such interaction-heavy scenarios performance may degrade significantly.

## References

Bae, I., Park, J.-H., and Jeon, H.-G. Learning pedestrian group representations for multi-modal trajectory prediction. In Avidan, S., Brostow, G., Cissé, M., Farinella, G. M., and Hassner, T. (eds.), *ECCV*, pp. 270–289, Cham, 2022. Springer Nature Switzerland.

Bae, I., Oh, J., and Jeon, H.-G. Eigentrajectory: Low-rank descriptors for multi-modal trajectory forecasting. In *Proceedings of the IEEE/CVF International Conference on Computer Vision (ICCV)*, pp. 10017–10029, October 2023.

Bae, I., Park, Y.-J., and Jeon, H.-G. Singulartrajectory: Universal trajectory predictor using diffusion model. In *Proceedings of the IEEE/CVF Conference on Computer Vision and Pattern Recognition (CVPR)*, pp. 17890–17901, June 2024.

Bhattacharyya, A., Hanselmann, M., Fritz, M., Schiele, B., and Straehle, C.-N. Conditional flow variational autoencoders for structured sequence prediction. In *NeurIPS*, 2019.

Chai, Y., Sapp, B., Bansal, M., and Anguelov, D. Multipath: Multiple probabilistic anchor trajectory hypotheses for behavior prediction. In Kaelbling, L. P., Kräig, D., and Sugiyama, K. (eds.), *Proceedings of the Conference on Robot Learning*, volume 100 of *Proceedings of Machine Learning Research*, pp. 86–99, 30 Oct–01 Nov 2020.

Chen, J., Cao, J., Lin, D., Kitani, K., and Pang, J. Mgf: Mixed gaussian flow for diverse trajectory prediction. In Globerson, A., Mackey, L., Belgrave, D., Fan, A., Paquet, U., Tomczak, J., and Zhang, C. (eds.), *NeurIPS*, volume 37, pp. 57539–57563. Curran Associates, Inc., 2024. doi: 10.52202/079017-1834.

Chen, K., Zhao, X., Huang, Y., Fang, G., Song, X., Wang, R., and Wang, Z. Socialmoif: Multi-order intention fusion for pedestrian trajectory prediction. In *CVPR*, pp. 22465–22475, June 2025.

Dai, B. et al. Diagnosing and preventing posterior collapse of vae. In *ICLR*, 2020.

Ettinger, S., Cheng, S., Caine, B., Liu, C., Zhao, H., Pradhan, S., Chai, Y., Sapp, B., Qi, C. R., Zhou, Y., Yang, Z., Chouard, A., Sun, P., Ngiam, J., Vasudevan, V., McCauley, A., Shlens, J., and Anguelov, D. Large scale interactive motion forecasting for autonomous driving: The waymo open motion dataset. In *ICCV*, pp. 9710–9719, October 2021.

Fang, Z., Hsu, D., and Lee, G. H. Neuralized markov random field for interaction-aware stochastic human trajectory prediction. In *The Thirteenth International Conference on Learning Representations*, 2025. URL <https://openreview.net/forum?id=r3cEOVj7Ze>.

Floreano, D. and Wood, R. J. Science, technology and the future of small autonomous drones. *nature*, 521(7553): 460–466, 2015.

Fu, Y., Yan, Q., Wang, L., Li, K., and Liao, R. Moflow: One-step flow matching for human trajectory forecasting via implicit maximum likelihood estimation based distillation. In *CVPR*, pp. 17282–17293, June 2025.

Gupta, A., Johnson, J., Fei-Fei, L., Savarese, S., and Alahi, A. Social gan: Socially acceptable trajectories with generative adversarial networks. In *Proceedings of the IEEE conference on computer vision and pattern recognition*, pp. 2255–2264, 2018.

HU, B. and Cham, T.-J. TSC-net: Prediction of pedestrian trajectories by trajectory-scene-cell classification. In *ICLR*, 2025. URL <https://openreview.net/forum?id=Xmh5gdMfRJ>.

Jang, E., Gu, S., and Poole, B. Categorical reparameterization with gumbel-softmax. In *International Conference on Learning Representations*, 2017.

Kingma, D. P. and Welling, M. Auto-encoding variational bayes. *arXiv preprint arXiv:1312.6114*, 2013.

Lee, N., Choi, W., Vernaza, P., Choy, C. B., Torr, P. H., and Chandraker, M. Desire: Distant future prediction in dynamic scenes with interacting agents. In *Proceedings of the IEEE conference on computer vision and pattern recognition*, pp. 336–345, 2017.

Lerner, A., Chrysanthou, Y., and Lischinski, D. Crowds by example. In *Computer graphics forum*, volume 26, pp. 655–664. Wiley Online Library, 2007.

Liang, J., Jiang, L., Murphy, K., Yu, T., and Hauptmann, A. The garden of forking paths: Towards multi-future trajectory prediction. In *Proceedings of the IEEE/CVF conference on computer vision and pattern recognition*, pp. 10508–10518, 2020.

Madjid, N. A., Ahmad, A., Mebrahtu, M., Babaa, Y., Nasser, A., Malik, S., Hassan, B., Werghi, N., Dias, J., and Khonji, M. Trajectory prediction for autonomous driving: Progress, limitations, and future directions. *arXiv preprint arXiv:2503.03262*, 2025.

Maeda, T. and Ukita, N. Fast inference and update of probabilistic density estimation on trajectory prediction. In *Proceedings of the IEEE/CVF International Conference on Computer Vision (ICCV)*, pp. 9795–9805, October 2023.

Mangalam, K., Girase, H., Agarwal, S., Lee, K.-H., Adeli, E., Malik, J., and Gaidon, A. It is not the journey but the destination: Endpoint conditioned trajectory prediction. In *European conference on computer vision*, pp. 759–776. Springer, 2020a.

Mangalam, K., Girase, H., Agarwal, S., Lee, K.-H., Adeli, E., Malik, J., and Gaidon, A. It is not the journey but the destination: Endpoint conditioned trajectory prediction. In Vedaldi, A., Bischof, H., Brox, T., and Frahm, J.-M. (eds.), *ECCV*, pp. 759–776, Cham, 2020b. Springer International Publishing.

Mao, W., Xu, C., Zhu, Q., Chen, S., and Wang, Y. Leapfrog diffusion model for stochastic trajectory prediction. In *CVPR*, pp. 5517–5526, June 2023a.

Mao, W., Xu, C., Zhu, Q., Chen, S., and Wang, Y. Leapfrog diffusion model for stochastic trajectory prediction. In *Proceedings of the IEEE/CVF conference on computer vision and pattern recognition*, pp. 5517–5526, 2023b.

Martín-Martín, R., Patel, M., Rezatofighi, H., Shenoi, A., Gwak, J., Frankel, E., Sadeghian, A., and Savarese, S. Jrdb: A dataset and benchmark of egocentric robot visual perception of humans in built environments. *IEEE Transactions on Pattern Analysis and Machine Intelligence*, 45(6):6748–6765, 2023. doi: 10.1109/TPAMI.2021.3070543.

Nicoli, K. A., Anders, C. J., Hartung, T., Jansen, K., Kessel, P., and Nakajima, S. Detecting and mitigating mode-collapse for flow-based sampling of lattice field theories. *Physical Review D*, 108(11):114501, 2023.

Panaretos, V. M. and Zemel, Y. Statistical aspects of wasserstein distances. *Annual review of statistics and its application*, 6(1):405–431, 2019.

Pellegrini, S., Ess, A., Schindler, K., and van Gool, L. You'll never walk alone: Modeling social behavior for multi-target tracking. In *2009 IEEE 12th International Conference on Computer Vision*, pp. 261–268, 2009. doi: 10.1109/ICCV.2009.5459260.

Phan-Minh, T., Grigore, E. C., Boulton, F. A., Beijbom, O., and Wolff, E. M. Covernet: Multimodal behavior prediction using trajectory sets. In *Proceedings of the IEEE/CVF Conference on Computer Vision and Pattern Recognition (CVPR)*, June 2020.

Robicquet, A., Sadeghian, A., Alahi, A., and Savarese, S. Learning social etiquette: Human trajectory understanding in crowded scenes. In *European conference on computer vision*, pp. 549–565. Springer, 2016.

Rudenko, A., Palmieri, L., Herman, M., Kitani, K. M., Gavrila, D. M., and Arras, K. O. Human motion trajectory prediction: a survey. *The International Journal of Robotics Research*, 39(8):895–935, 2020. doi: 10.1177/0278364920917446.

Sadat, A., Casas, S., Ren, M., Wu, X., Dhawan, P., and Urtasun, R. Perceive, predict, and plan: Safe motion planning through interpretable semantic representations. In *ECCV*, pp. 414–430, 2020.

Salzmann, T., Ivanovic, B., Chakravarty, P., and Pavone, M. Trajectron++: Dynamically-feasible trajectory forecasting with heterogeneous data. In Vedaldi, A., Bischof, H., Brox, T., and Frahm, J.-M. (eds.), *ECCV*, pp. 683–700, Cham, 2020. Springer International Publishing.

Shi, L., Wang, L., Zhou, S., and Hua, G. Trajectory unified transformer for pedestrian trajectory prediction. In *Proceedings of the IEEE/CVF International Conference on Computer Vision (ICCV)*, pp. 9675–9684, October 2023.

Shi, S., Jiang, L., Dai, D., and Schiele, B. Mtr++: Multi-agent motion prediction with symmetric scene modeling and guided intention querying. *IEEE Transactions on Pattern Analysis and Machine Intelligence*, 46(5):3955–3971, 2024.

Sohn, K., Lee, H., and Yan, X. Learning structured output representation using deep conditional generative models. In Cortes, C., Lawrence, N., Lee, D., Sugiyama, M., and Garnett, R. (eds.), *Advances in Neural Information*

*Processing Systems*, volume 28. Curran Associates, Inc., 2015.

Sun, J., Li, Y., Fang, H.-S., and Lu, C. Three steps to multimodal trajectory prediction: Modality clustering, classification and synthesis. In *ICCV*, pp. 13250–13259, October 2021.

Yan, C., Wang, S., Yang, J., Xu, T., and Huang, J. Re-balancing variational autoencoder loss for molecule sequence generation. In *Proceedings of the 11th ACM international conference on bioinformatics, computational biology and health informatics*, pp. 1–7, 2020.

## A. Theoretical Proofs

In this section, we provide rigorous proofs for the theoretical framework presented in Section 3. We treat future trajectories  $Y_j$  as continuous random variables in  $\mathbb{R}^{T_{\text{pred}} \times d}$ .

### A.1. Proof of Theorem 3.1

**Theorem 3.1.** Define the distribution matching loss as the KL divergence  $\mathcal{L}_{\text{dist}}(X) = \text{KL}(p(Y_j|X) \| q(Y_j|X))$ . The loss is lower-bounded by the gap between prior mismatch  $\epsilon_{\text{prior}}$  and sampler error  $\epsilon_{\text{sample}}$ :

$$\mathcal{L}_{\text{dist}}(X) \geq \frac{1}{2} (\epsilon_{\text{prior}}(X) - \epsilon_{\text{sample}}(X))^2. \quad (37)$$

*Proof.* By **Pinsker's Inequality**, the KL divergence between two distributions  $p$  and  $q$  is bounded by their Total Variation (TV) distance, or equivalently, their  $L_1$  norm:

$$\mathcal{L}_{\text{dist}}(X) \geq 2\|p(Y_j|X) - q(Y_j|X)\|_{\text{TV}}^2 = \frac{1}{2}\|p(Y_j|X) - q(Y_j|X)\|_1^2. \quad (38)$$

To decompose the error, we introduce an auxiliary distribution  $\tilde{q}(Y_j|X) = \int p(z|X)q(Y_j|X, z) dz$ , which represents the output of the current sampler under a *perfect* prior. The  $L_1$  term can be expanded as:

$$\begin{aligned} \Delta &= \|p(Y_j|X) - q(Y_j|X)\|_1 \\ &= \|(p(Y_j|X) - \tilde{q}(Y_j|X)) + (\tilde{q}(Y_j|X) - q(Y_j|X))\|_1. \end{aligned} \quad (39)$$

Applying the Reverse Triangle Inequality ( $\|A + B\|_1 \geq \|\|A\|_1 - \|B\|_1\|$ ), we have:

$$\Delta \geq \|\tilde{q}(Y_j|X) - q(Y_j|X)\|_1 - \|p(Y_j|X) - \tilde{q}(Y_j|X)\|_1. \quad (40)$$

By definition from the main text:

$$\epsilon_{\text{prior}}(X) = \|\tilde{q} - q\|_1 = \left\| \int (p(z|X) - q(z|X))q(Y_j|X, z) dz \right\|_1, \quad (41)$$

$$\epsilon_{\text{sample}}(X) = \|p - \tilde{q}\|_1 = \left\| \int p(z|X)(p(Y_j|X, z) - q(Y_j|X, z)) dz \right\|_1. \quad (42)$$

Substituting these into Eq. (38) yields:

$$\mathcal{L}_{\text{dist}}(X) \geq \frac{1}{2} (|\epsilon_{\text{prior}}(X) - \epsilon_{\text{sample}}(X)|)^2 = \frac{1}{2} (\epsilon_{\text{prior}}(X) - \epsilon_{\text{sample}}(X))^2. \quad (43)$$

□

### A.2. Proof of Proposition 3.2

*Proof.* For trajectory  $Y_j$  of total dimension  $D = T_{\text{pred}} \times d$ , the reconstruction error of any sampler is bounded by the prior. Specifically, for any latent variable  $z$ , the Mean Squared Error (MSE) satisfies:

$$\text{MSE}(Y_j, \hat{Y}_j) \geq \frac{D}{2\pi e} \exp\left(\frac{2}{D} H(Y_j|X, z)\right), \quad (44)$$

where  $H(\cdot)$  denotes the differential entropy. Using the identity  $H(Y_j|X, z) = H(Y_j|X) - I(Y_j; z|X)$ , we obtain:

$$\text{MSE}(Y_j, \hat{Y}_j) \geq \frac{D}{2\pi e} \exp\left(\frac{2}{D} [H(Y_j|X) - I(Y_j; z|X)]\right). \quad (45)$$

Since the  $L_1$  sampler error  $\epsilon_{\text{sample}}$  is lower-bounded by the square root of the MSE (up to a scaling factor  $\kappa$  depending on the distribution shape), we define the bound function  $\mathcal{C}(\cdot)$  as:

$$\mathcal{C}(I) = \kappa \cdot \sqrt{\frac{D}{2\pi e}} \exp\left(\frac{1}{D}[H(Y_j|X) - I]\right). \quad (46)$$

As  $I(Y_j; z|X)$  decreases (i.e., the prior captures less information),  $\epsilon_{\text{sample}}$  is forced to increase exponentially, establishing the sampler's performance ceiling.  $\square$

### A.3. Proof of Corollary 3.3

*Proof.* We consider the case where  $\epsilon_{\text{prior}} > \epsilon_{\text{sample}}$ , a standard condition in multimodal forecasting where mode loss dominates fitting noise. In this regime, the term inside the square of Theorem 3.1 is positive.

To achieve a target matching accuracy  $\mathcal{L}_{\text{dist}}(X) < \delta$ , we must satisfy:

$$\begin{aligned} \frac{1}{2}(\epsilon_{\text{prior}}(X) - \epsilon_{\text{sample}}(X))^2 &< \delta \\ \epsilon_{\text{prior}}(X) - \epsilon_{\text{sample}}(X) &< \sqrt{2\delta}. \end{aligned} \quad (47)$$

Rearranging for  $\epsilon_{\text{prior}}$  and substituting the absolute lower bound for the sampler error  $\epsilon_{\text{sample}}^{\min}$  from Proposition 3.2:

$$\epsilon_{\text{prior}}(X) < \sqrt{2\delta} + \epsilon_{\text{sample}}^{\min}(X). \quad (48)$$

This indicates that even with an optimal sampler ( $\epsilon_{\text{sample}} \rightarrow \epsilon_{\text{sample}}^{\min}$ ), the distribution error  $\delta$  cannot be reduced unless the prior mismatch  $\epsilon_{\text{prior}}$  is strictly controlled, proving that high-quality priors are a *necessary* condition for accurate multimodal forecasting.  $\square$

## B. Application in Batch Clustering

When building the binary adjacency matrix  $A_{ij}$  in Section 4.2, we rely on hard thresholding conditions:

$$A_{ij} = \mathbb{I}[\tilde{S}_{ij} > \theta_{\text{sim}}] \wedge \mathbb{I}[\tilde{R}_{ij} < \theta_{\text{rep}}]$$

The indicator function  $\mathbb{I}[\cdot]$  is non-differentiable. To enable end-to-end training, we approximate these hard choices using sigmoid functions with temperature parameters:

$$\hat{A}_{ij} = \text{sigmoid}\left(\frac{(\tilde{S}_{ij} - \theta_{\text{sim}})}{\tau_{\text{sim}}}\right) \cdot \text{sigmoid}\left(\frac{(\theta_{\text{rep}} - \tilde{R}_{ij})}{\tau_{\text{rep}}}\right)$$

where  $\tau_{\text{sim}}$  and  $\tau_{\text{rep}}$  are temperature parameters. During training, we use  $\tau_{\text{sim}} = \tau_{\text{rep}} = 0.1$  to approximate hard thresholding while maintaining differentiability. This allows backpropagation through the graph construction, enabling joint learning of feature projections and thresholds.

## C. Application in Global Prior Sampling

In Section 4.3, agent  $(b, j)$  obtains attention weights  $\mathbf{a}_{b,j} = \{\alpha_{b,j,g}\}_{g=1}^{K_g}$  over global GMM components. To sample from this discrete distribution while maintaining differentiability, we apply Gumbel-Softmax:

$$\tilde{z}_{b,j,g}^{(n)} = \frac{\exp((\log \alpha_{b,j,g} + G_g^{(n)})/\tau)}{\sum_{j'=1}^{K_g} \exp((\log \alpha_{b,j,j'} + G_{j'}^{(n)})/\tau)}$$

where  $G_g^{(n)} \sim \text{Gumbel}(0, 1)$  and  $\tau$  is the temperature parameter.

We set  $\tau = 1.0$  to maintain multimodality during sampling. This higher temperature prevents mode collapse by allowing the sampled vector  $\tilde{\mathbf{z}}_{b,j}^{(n)}$  to be "soft" (non-one-hot), reflecting the underlying distribution  $\mathbf{a}_{b,j}$  and encouraging exploration of multiple plausible modes simultaneously.

## D. Implementation Details

We implement AGMA using PyTorch. In the following, we detail the network architecture, hyperparameters, and specific algorithmic settings derived from our official implementation.

### D.1. Network Architecture

The model processes the observed trajectories of length  $T_{\text{obs}} = 8$  and predicts future trajectories of length  $T_{\text{pred}} = 12$ , with a hidden core dimension  $d = 32$ . Both history and future encoders utilize a spatio-temporal encoder with self-attention, where spatial coordinates are first embedded via MLPs before being processed by the encoder. Similarity and repulsion heads ( $\Phi_{\text{sim}}$ ,  $\Phi_{\text{rep}}$ ) are implemented as 2-layer MLPs with sigmoid activation to output probabilities in  $[0, 1]$ . To query the global prior, we employ an attention mechanism where the query is the past feature and the key is a concatenation of global centroids, covariances, and weights. We utilize Entmax1.5 (?)—a sparse alternative to softmax—to compute attention scores, encouraging the model to attend to a sparse set of relevant global modes. The sampled latent codes are refined using multi-head attention with 4 heads and an embedding dimension of  $20 \times d$ , allowing interaction modeling between the  $N = 20$  samples.

### D.2. Hyperparameters and Settings

**Global and Batch Priors.** We set the number of global Gaussian components to  $K_g = 100$ , with centroids and covariances initialized from a normal distribution. The similarity threshold  $\theta_{\text{sim}}$  and the repulsion threshold  $\theta_{\text{rep}}$  are initialized as learnable parameters at 0.7 and 0.3, respectively. The temperature parameter  $\tau$  used in the Gumbel-Softmax and Straight-Through Estimator is set to 0.1, which encourages sharper decision boundaries for clustering and mode selection.

**Optimal Transport (Sinkhorn).** For the global-to-batch distillation stage, we solve the optimal transport problem using the Sinkhorn-Knopp algorithm with 20 iterations to approximate the optimal assignment matrix  $\mathbf{P}$ . The cost matrix between the global component  $g$  and the batch component  $b$  is defined as the 2-Wasserstein distance approximation:  $C_{gb} = \|\mu_g - \mu_b\|^2 + \|\sigma_g - \sigma_b\|_F^2$ , where the second term represents the trace of squared differences of standard deviations.

**Training Configuration.** We sample  $N = 20$  trajectories for both training and evaluation. The model is trained using the AdamW optimizer, with the total loss comprising student predictions (from the global prior), teacher predictions (from the batch prior), and the distillation loss.